Simple and inexpensive electrodeposited silver/polyaniline composite counter electrodes for dye-sensitized solar cells

Sheeba Ghani · Rehana Sharif · Shamaila Shahzadi ·
N. Zafar · A. W. Anwar · Ayesha Ashraf · Azhar A. Zaidi ·
Afzal H. Kamboh · Saima Bashir

Abstract Silver and polyaniline (Ag/PANI) composite counter electrodes (CEs) have been prepared by electrochemical polymerization on stainless steel substrate using different silver (Ag) concentrations for dye-sensitized solar cells (DSSC). The effect of Ag concentration on the properties of fabricated Ag/PANI composite CEs, such as morphology, electrical conductivity, oxidation and reduction potential, and electrochemical activity of I_3^- reduction, is investigated. Highest cathodic current density (3.4 mA), low charge transfer resistance (2.15 Ω), and good electrocatalytic activity of I_3^-/I^- redox couple for CE are obtained at 0.07 M concentration of silver in Ag/PANI composite. DSSC based on this CE shows best photovoltaic performance with conversion efficiency up to 7.31 %. This study indicates that the Ag/PANI composite prepared electrochemically is possible substitute of the expensive Platinum as CEs for DSSCs.

S. Ghani (✉) · R. Sharif · S. Shahzadi · N. Zafar ·
A. W. Anwar · A. Ashraf · A. A. Zaidi · S. Bashir
Department of Physics, University of Engineering and
Technology, Lahore, Pakistan
e-mail: sheeba.ghani@yahoo.com

A. H. Kamboh
Pakistan Council of Renewable Energy Technologies,
Islamabad, Pakistan

Introduction

Dye-sensitized solar cells (DSSCs) are of great attention among solar cells due to low cost and high photovoltaic efficiency. The DSSC is composed of dye-sensitized TiO_2 photo electrode, a counter electrode (CE), and I_3^-/I^- redox electrolyte solution. The CE is key component in DSSC, which is used to shift electrons from outer circuit to the electrolyte solution and to reduce the triiodide ions (I_3^-) to Iodide ions (I) [1–4]. Generally, a thin platinum (Pt) film deposited on transparent conductive oxides (TCO) glass is widely adopted as CE in DSSC for the reduction of I_3^-. However, Pt CE is expensive and restricts its use at commercial scale DSSC [5, 6]. To reduce the fabrication cost of DSSC, it is required to adopt cost-effective alternative materials such as carbonous materials, conducting polymers, and their composites for CEs [7–17].

Among conducting polymers, polyaniline (PANI) is the most attractive material to replace Pt CE because of its easy synthesis, considerable catalytic activity, and good environmental stability [18, 19]. Li et al. [20], Qin et al. [21], and Xiao et al. [22] use electrochemically polymerized Polyaniline film on ITO glass as a counter electrode for DSSC and achieve a conversion efficiency up to 5.8 % with smaller charge transfer resistance and higher electrolyte catalytic activity of I_3^-/I^- redox reaction. Typically, PANI has conductivity of the order of 1 S cm^{-1}. The coupling of metals with PANI is the most suitable choice to enhance its conductivity [23, 24].

The platinum nano-particle (PtNP)/PANI composite-based CEs have been investigated and exhibit unique properties of both PtNP and PANI. Higher conductivity is observed for the PtNP/PANI composite CE as compared to the PtNP and PANI CE. Consequently, PtNP/PANI composite-based DSSC showed better PV performance than the PANI and the

Pt-based DSSCs [25, 26]. Many efforts have been made to synthesize other materials for the CEs using conducting polymer/metal composites. Since silver has high conductivity among all the metals, the incorporation of silver into PANI may enhance electrical and catalytic properties [27, 28]. A recent research by A.B.V. Kiran Kumar et al. has been focused on replacing ITO by Ag nanowire/PANI composite film for transparent electrodes because of their preferred conducting and optical properties [29]. In this study, Ag/PANI composite films are formed on stainless steel (SS) 304 substrate using electropolymerization technique. The electropolymerization method is simple and cost-effective to synthesize Ag/PANI composite films with good adhesion to the substrate and controllable surface morphology as compared to chemical polymerization [11]. The Ag/PANI composite as counter electrode for DSSC has not been studied earlier. The novelty of this work is the fabrication Ag/PANI composite CEs and the sequential investigation of morphology and conductivity of composite films along with the photoelectric performance of DSSC. This research describes a simple way to enhance the electrical and electrochemical properties of polyaniline doped with metal as a CE for DSSC.

Preparation of Silver/PANI composite CE

All electro-polymerization tests were performed in one compartment cell using three-electrode arrangement on Princeton 263A electrochemical work station. A graphite electrode (1 cm^2), SS 304 sheet, and saturated calomel electrode (SCE) were used as counter electrode, working electrode, and reference electrode, respectively. The SS sheet is mechanically polished with fine emery paper and then rinsed with double-distilled water in an ultrasonic bath before using. The working area of the SS was 1 cm^2.

Three electrodes were immersed in aqueous solution containing 0.2 M aniline, 0.01–0.1 M AgNO$_3$, and 0.2 M H$_2$SO$_4$. Ag/PANI composite was deposited on SS sheet at 1.0 V versus SCE. The prepared samples were AgPANI-1, AgPANI-2, AgPANI-3, AgPANI-5, AgPANI-7, and AgPANI-10 having AgNO$_3$ concentration of 0.01, 0.02, 0.03, 0.05, 0.07, and 0.1 M, respectively. A green film gradually formed on the SS sheet and becomes dark with the passage of time. The thickness of the film was measured and controlled by the amount of charge transfer between the electrode and the solution. In this work, the film thickness of Ag/PANI composite films was approximately 1 μm. After deposition, Ag/PANI Composite CE electrode was immersed in 0.5 M H$_2$SO$_4$ at 0.4 V versus SCE for 2 min to remove aniline monomer from the composite polymeric film. The Ag/PANI Composite CE was washed with distilled water and desiccated at 70 °C for 24 h. A pure PANI film was also deposited on SS using the same method without the addition of AgNO$_3$. The thickness and morphology of Ag/PANI Composite CEs were adequately controlled by the

precise control of the reaction conditions (time, concentration, temperature, and deposited charge).

Fabrication of DSSCs

The following procedure was used to fabricate photoanode of DSSC. Firstly, a thin TiO$_2$ blocking layer was deposited on FTO substrate by immersing in 50 mM TiCl$_4$ isopropanol solution at 70 °C for 30 min. Secondly, the TiO$_2$ Colloid was prepared by mixing 2 g TiO$_2$ (P25) powder, 4 mL DI (deionized water), 0.8 mL acetylacetone, and 0.1 mL Triton X. The mixture was stirred ultrasonically for two hours. The TiO$_2$ colloid was coated on the TiO$_2$-blocking layer using doctor blade method and sintered at 450 °C for 30 min. After cooling, the TiO$_2$ anode was immersed in 0.5 mM solution of N719 dye in a mixture of acetonitrile/tert-butanol (volume ratio 1:1) for 24 h. Finally, a DSSC was fabricated by injecting a drop of redox electrolyte (0.1 M LiI, 0.05 M I$_2$, 0.6 M tetra butylammonium Iodide, and 0.5 M tert-butyl pyridine in acetonitrile) in the aperture between photoanode and CE, made from PANI and Ag/PANI composite, and for comparison, a thermally decompose Pt on SS is also used as CE [30].

Characterizations and measurements

The electrical conductivity of PANI and Ag/PANI samples was measured by four-probe method using a current source SMU Keithley 237 and a Multimeter Keithley 2010. The X-ray diffractogram of the samples was obtained by 2001 Bruker-AXS diffractrometer using CuK$_\alpha$ radiation. The surface morphologies of CEs were observed using a scanning electron microscopy (SEM; JSM-6480LV). Cyclic voltametry was performed on Princeton 263A electrochemical work station using three-electrode system. The graphite electrode, saturated calomel electrodes, and PANI and Ag/PANI were used as counter, reference, and working electrodes. The electrolyte was acetonitrile solution consisting of 10 mM LiI, 1 mM I$_2$ as I$_3^-$/I$^-$ redox couple, and 0.1 M LiClO$_4$ as supporting electrolyte [31–33]. The Tafel polarization measurements were performed using a symmetric cell made of two identical CEs at a scan rate of 10 mV/s using the same electrolyte as that for DSSC. The photovoltaic efficiency of DSSC was measured under 100 mW/cm^2 from a solar simulator (HAL-C100).

Results and discussion

Silver/PANI composite formation

In electrochemical synthesis, aniline monomer and silver nitrate in sulfuric acid solution are treated electrochemically
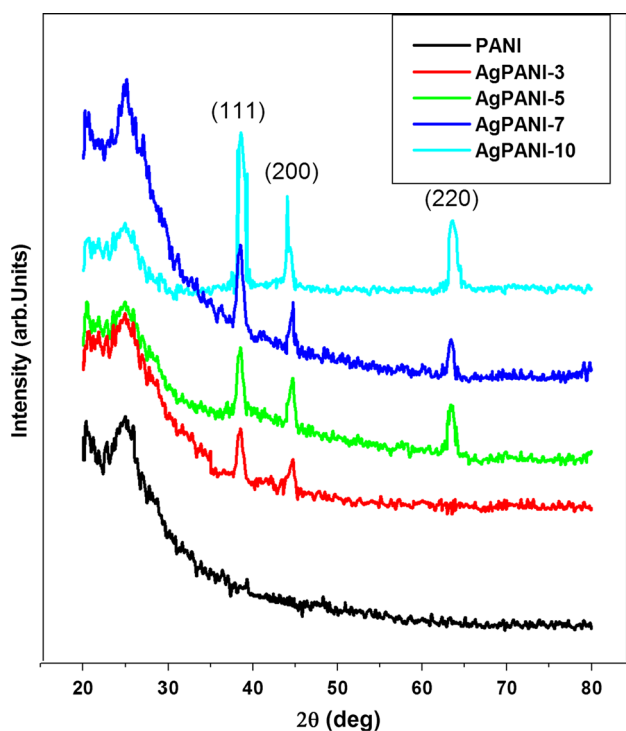
Fig. 1 XRD spectra of PANI and Ag/PANI composite

to produce silver particles embedded in PANI film. Aniline is oxidized with silver nitrate to polyaniline while metallic silver and nitric acid are reaction by-products. A part of H_2SO_4 is neutralized by aniline to form PANI and reduce the acidity of the medium, which acts against the polymerization of aniline. This decrease in acidity is compensated by the nitric acid generated during the oxidation of aniline by silver nitrate. Nitric acid supports aniline oxidation and adjusts the acidity of the medium [34–36].

PANI produced during the oxidation of aniline is also able to reduce silver ions to metallic silver. Based upon the above prospective, two silver reductants, a monomer (aniline) and a polymer (PANI), are always present in the reaction mixture [37]. A simple redox reaction between PANI and the silver salt becomes complicated in the presence of two reductants of silver ions.

Structural characterization

The crystalline nature of the Ag/PANI composite is determined by XRD analysis as shown in Fig. 1. The diffraction peaks at $2\theta = 38.54°$, $44.9°$, and $63.5°$ represent the cubic structure of Ag for the diffraction planes (111), (200), and (220), respectively. All the peaks are indexed to face-centered cubic structure [38]. The diffraction peaks confirm the incorporation of metallic silver particles in the composites and their crystalline nature. This result is well matched with standard spectrum of crystalline silver

(JCPDS NO. 4-0783). XRD analysis confirms that the silver particles are embedded within the PANI matrix. The XRD patterns clearly indicate that intensity of peaks has been increased as the concentration of the silver is increased from 0.03 to 0.1 M.

The two peaks at low diffraction angle centered at $2\theta = 20.3°$ and $24.7°$ show periodicity parallel and perpendicular to polymer chain, respectively [39]. The sharpness of these peaks denotes the degree of alignment of PANI chains, and the intensity shows the population of crystallites in that particular plane [40]. But in the present case, these two peaks are not sharp due to the poor orientation of PANI chains.

Morphological study

The surface morphology of PANI is shown in Fig. 2a. The surface of PANI film is quite rough because the electrochemical polymerization of PANI from aniline is a two-stage growth process. Firstly, a dense and compact layer of PANI appeared on the bare electrode and then PANI grows anisotropically to form a loosely bound structure [41, 42].

The content of metallic silver in Ag/PANI composite is found to be 18, 13, 9, and 7 wt % for AgPANI-10, AgPANI-7 AgPANI-5, and AgPANI-3, respectively, determined from energy-dispersive X-ray spectroscopy. Figure 2b–e is the SEM images of AgPANI-3, AgPANI-5, AgPANI-7, and AgPANI-10, respectively. In Fig. 2b, the white spots are the silver particles that bound to the polyaniline matrix due to firm affinity of silver for nitrogen. It is also observed that the spherical-shaped silver particles are uniformly dispersed in the PANI matrix. These particles are monodispersed at low concentration. The average diameter of silver particles is 200–250 nm; since the silver particles are created in the polyaniline solution, the particles are embedded in the PANI matrix [43]. The formation of relatively large Ag clusters is associated with the agglomeration of Ag particles for high silver concentration as shown in Fig. 2c. The agglomeration of particles is due to their high surface energy. Their agglomeration creates thermodynamically stable clusters [44, 45]. The porous surface with uniformly distributed silver particles is observed in Fig. 2d. This uniform porosity is an essential parameter for electrocatalytic activity. A honeycomb structure rather than distinct silver particles is observed in Fig. 2e for sample AgPANI-10.

Conductivity of silver/PANI composite

The conductivity of the Ag/PANI composite films is studied by four-probes measurement system and calculated by the following equation:

Fig. 2 SEM micrographs of **a** PANI, **b** AgPANI-3, **c** AgPANI-5, **d** AgPANI-7, and **e** AgPANI-10. The **a***, **b***, **c***, **d***, and **e*** are the respective magnified images
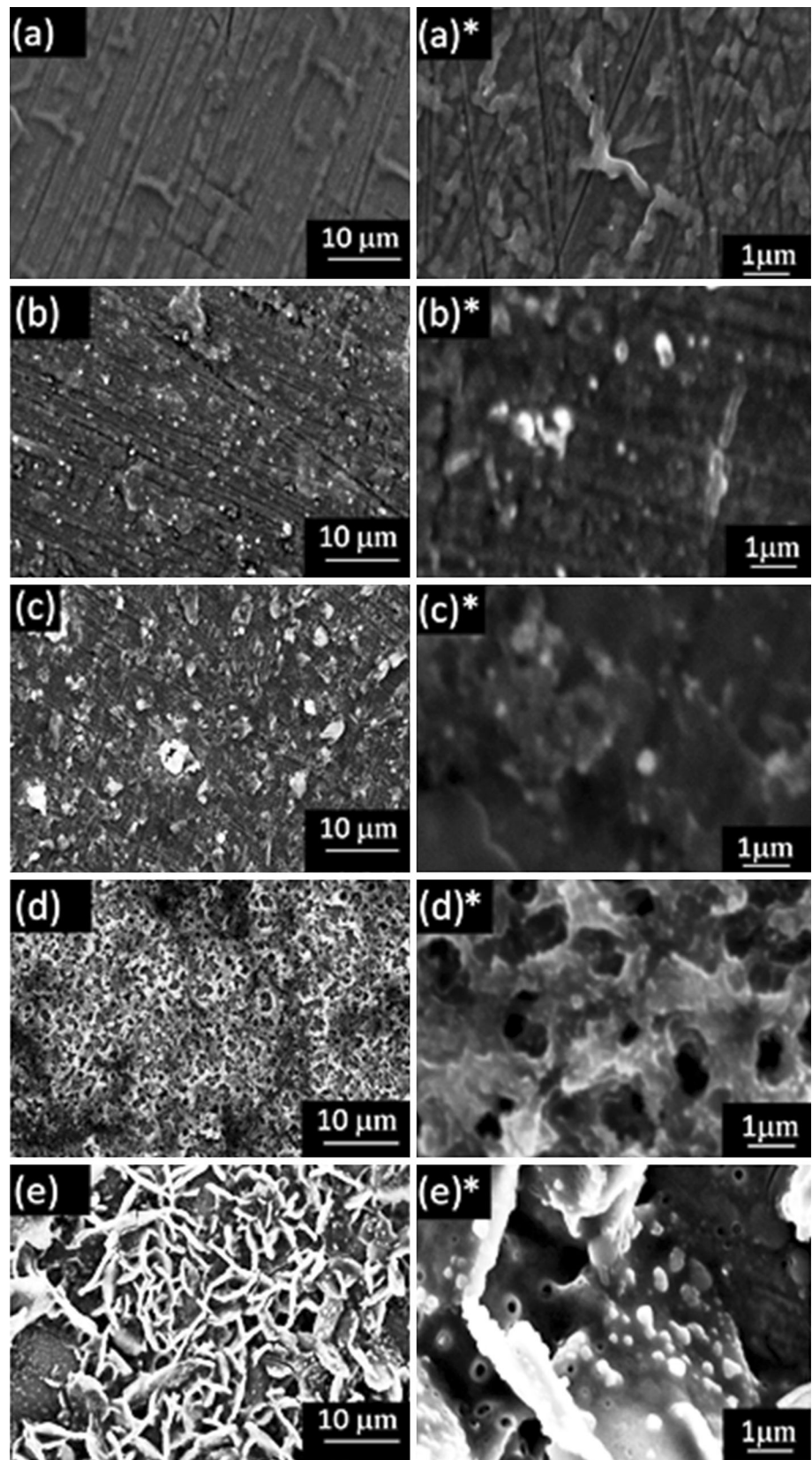
Table 1 Conductivity of PANI and Ag/PANI films using different AgNO₃ concentrations

Electrodes	AgNO₃ (M)	Conductivity (S cm⁻¹)
PANI	0	10.42
AgPANI-1	0.01	13.48
AgPANI-2	0.02	17.8
AgPANI-3	0.03	30.56
AgPANI-5	0.05	44.28
AgPANI-7	0.07	67.74
AgPANI-10	0.1	89.23

$$\sigma = \ln 2 / \pi d * I/U, \tag{1}$$

where σ is the conductivity, d is the thickness of the film, which is 1 μm, and I and U are the current and potential difference, respectively [21]. The sample code and the conductivity of the Ag/PANI composite films with different concentrations of AgNO₃ are given in Table 1. The electrical conductivity of Ag/PANI composite is higher than pure PANI film and increases with the increase of silver content in the Ag/PANI composite. The lower conductivity of pure PANI is due to its amorphous nature as indicated in XRD pattern. The crystalline nature of silver particles forms ordered structure in the composite films, which permits improved electrical transport [46, 47].

Electrochemical measurements

Figure 3 shows the cyclic voltammetry curves of I_3^-/I^- redox couple on the CEs. The anodic current peak represents oxidation, and cathodic current peak is related to reduction [11, 48]. Table 2 shows cathodic peak current (I_{Pc}), cathodic peak potential (E_{Pc}), and peak to peak seperation (E_{pp}) data for PANI, Ag/PANI composite, and Pt CEs. The reaction occurs on the CE of DSSC is the reduction of I_3^-/I^- redox couple, and thus only cathodic reaction is considered. The CV curves indicate that the cathodic current density of I_3^-/I^- redox couple for Ag/PANI composite CEs is higher than PANI CE which shows a rapid reaction rate and low charge transfer resistance of I_3^-/I^- redox couple on the Ag/PANI composite CEs. The cathodic current densities are gradually increased with Ag concentration, and the reductive peaks shift to more positive potentials. The E_{pp} value (shown in Table 2) decreases in the order of PANI (556 mV) > AgPANI-3 (537mv) > AgPANI-5(524 mV) > AgPANI-10(518 mV) > Pt (480 mV) > AgPANI-7 (474 mV), whereas J_{sc} increases in the order of Pt > AgPANI-7 > AgPANI-10 > AgPAN-5 > AgPANI-3, representing the same order of electrocatalytic activity. Moreover, the cathodic peak potential (E_{Pc}) of AgPANI-7 and Pt electrode is almost equal but more positive than other CEs fabricated in the present work. This indicates that the over potential for
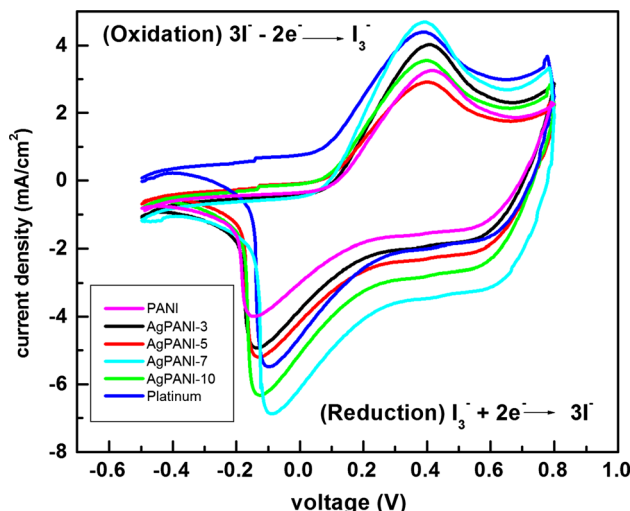

Fig. 3 Cyclic voltametry curves of various CEs at scan rate of 50 mV/sec

Table 2 Cyclic voltametry and Tafel polarization measurements of different CEs

CE	I_{pc} (mA cm⁻²)	E_{pc}(V)	E_{pp}(V)	J_o (mA cm⁻²)	R_{ct} (Ω cm⁻²)
PANI	2.5	−0.143	0.556	5.33	2.41
AgPANI-3	2.8	−0.133	0.537	5.35	2.40
AgPANI-5	2.9	−0.127	0.524	5.71	2.25
AgPANI-7	3.4	−0.086	0.474	5.97	2.15
AgPANI-10	3.3	−0.124	0.518	5.85	2.19
Platinum	3.5	−0.095	0.480	6.00	2.14

reduction of I_3^- to I^- for AgPANI-7 and Pt electrode is much smaller. A small E_{pp} value and a large I_{pc} are also observed when AgPANI-7 has been used as CE. Thus, AgPANI-7 has the highest electrocatalytic activity of I_3^-/I^- redox couple, which is equivalent to the Pt electrode, and it can be a substitute of Pt CE in DSSC [49].

To investigate the charge transfer properties of I_3^-/I^- redox couple on CE surface, Tafel polarization measurement is performed on symmetric cells using two similar electrodes with the same electrolyte as used in DSSC. Figure 4 shows the Tafel measurement with logarithmic current density (log J) as a function of voltage (V) at 25 C⁰. Theoretically, the Tafel polarization curves can be separated into three zones [50]. The curve at very high potential >0.6 V is assigned to the limiting diffusion zone which relates to the diffusion coefficient of I_3^-/I^- redox couple in DSSC, given by Eq. (2), where J_{lim} is the limiting current density.

$$D = 1/2nFc * J_{lim} \tag{2}$$

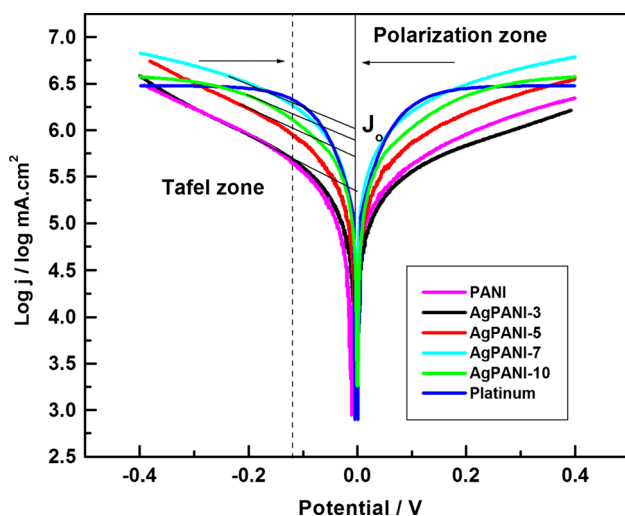$$V = 2.3RT(\lg j - \lg j_o)/\alpha nF \tag{3}$$

$$J_o = RT/nFR_{ct} \tag{4}$$

Fig. 4 Tafel curves of various symmetric cells

Fig. 5 Photocurrent-voltage curves of DSSCs using various CEs under standard illumination

The current at very low potential is assigned to polarization zone that originates from the electrochemical reaction, while curve at comparatively low potential >0.01 V is related to the Tafel zone, and voltage (V) is given by Eq. (3). In these equations, R is the universal gas constant, T is the temperature, j_0 is the exchange current density, F is the Faraday 's constant, α is the distribution coefficient, and n ($n = 2$) is the number of electrons involved in the reaction [51, 52].

The slopes of the curves in the Tafel zone for cathodic or anodic branches are in the order of pt > AgPANI-7 > AgPANI-10 > AgPANI-5 > AgPANI-3 > PANI. A steep slope indicates higher J_0 that suggests large surface area and higher conductivity which is an important factor for large catalytic activity [53]. J_0 is related to R_{ct} by Eq. (4) and calculated from the Tafel curves in Fig. 5. R_{ct} is the charge transfer resistance for I_3^- reduction at the electrolyte/CE interface. Apparently, the measured J_0 value also shows the order of Pt > AgPANI-7 > AgPANI-10 > AgPANI-5 > AgPANI-3 > PANI, and R_{ct} shows the order of PANI > AgPANI-3 > AgPANI-5 > AgPANI-10 > AgPANI-7 > Pt. Thus, a CE with small R_{ct} indicates less overpotential for an electron moving from CE surface to the electrolyte. A small R_{ct} implies facile electron movement, while higher R_{ct} indicates sluggish electron transfer.

The R_{ct} of the Ag/PANI composite CEs decreases with increasing concentration of silver. The lowest R_{ct} value of 2.15 Ω cm^2 for AgPANI-7 CE is obtained when silver concentration is 0.07 M, which is comparable to that of Pt CE (2.14 Ω cm^2). Moreover, R_{ct} increases by increasing the amount of silver due to poor electrocatalytic activity of Ag/PANI composite CE. A decrease in R_{ct} value represents an increase in current density. AgPANI-7 CE with R_{ct}
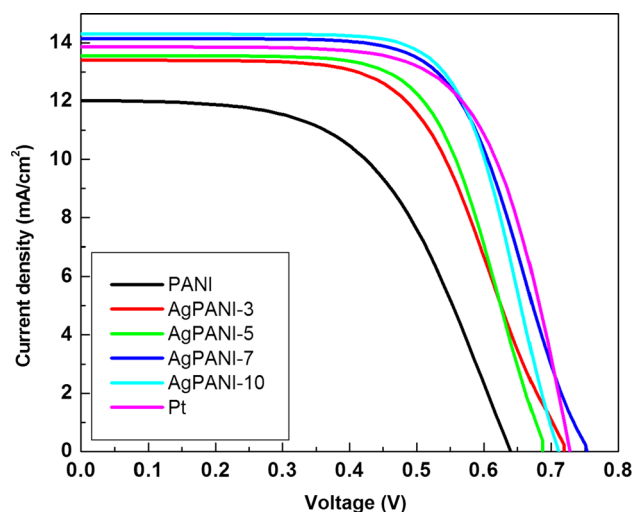
value of 2.15 Ω cm^2 has an exchange current density of 5.97 mA, whereas pure PANI CE has R_{ct} value of 2.48 Ω cm^2 corresponding to an exchange current density of 5.33 mA.cm^2. The CE prepared with concentration of 0.07 M of silver shows the lowest R_{ct} and the highest J_0, compared to other CEs. Thus, it shows highest electrocatalytic activity, which is in accordance with the CV result.

Photovoltaic characteristics of DSSC

Figure 5 shows the photovoltaic parameters of DSSCs using pure PANI and Ag/PANI composite CEs under light intensity of 100 mWcm^{-2}. The related photovoltaic parameters are listed in Table 3, which shows that DSSCs employing Ag/PANI composite CEs exhibit enhanced photovoltaic efficiency as compared to pure PANI CE. In fact, the DSSC made from AgPANI-7CE reveals short-circuit current density (J_{sc}), open-circuit voltage (V_{oc}), and fill factor (FF) of 14.91 mA cm^{-2}, 0.769 V, and 0.629, respectively, generating its photovoltaic efficiency 7.31 %, which is greater than 4.23 % for pure PANI electrode. The Ag/PANI composite CEs show much higher fill factor and photovoltaic efficiency, which display comparable short-circuit current density and open-circuit voltage than PANI CE. Such performance improvement is mainly due to higher electrocatalytic activity and large conductivity of Ag/PANI composite CEs [26].

All the DSSCs are made from the same TiO$_2$ photoanode, dye, and liquid electrolyte; therefore, the measured V_{oc} values are comparable. Generally, the V_{oc} value was determined from the difference between the Fermi level of the electron in TiO$_2$ and the formal potential of the redox couples on the CE [2, 54]. The J_{sc} value of AgPANI-7 CE is higher among all

Table 3 Photovoltaic parameters of DSSCs with different CEs

Electrodes	J_{sc} (mA cm^{-2})	V_{oc} (V)	FF	η (%)
PANI	12.1 ± 0.31	0.640 ± 0.02	0.547 ± 0.02	4.24 ± 0.24
AgPANI-3	13.4 ± 0.35	0.727 ± 0.04	0.595 ± 0.04	5.82 ± 0.34
AgPANI-5	13.5 ± 0.21	0.686 ± 0.12	0.662 ± 0.03	6.14 ± 0.23
AgPANI-7	14.9 ± 0.34	0.769 ± 0.01	0.629 ± 0.01	7.31 ± 0.35
AgPANI-10	14.3 ± 0.22	0.712 ± 0.23	0.692 ± 0.02	7.03 ± 0.22
Pt	13.9 ± 0.45	0.727 ± 0.10	0.703 ± 0.03	6.84 ± 0.32

CEs due to the high conductivity and good dispersion of silver particles into PANI matrix, which gives larger active surface areas for triiodides reduction, as mentioned in the CV tests. In addition, the value of R_{ct} plays a major role in FF of the DSSCs which are made of the identical photoanodes and liquid electrolyte but with different CEs. [55]. The R_{ct} of the Ag/PANI electrode is found to be smaller than PANI electrode as presented in Table 2. Therefore, the DSSC with Ag/PANI CE shows higher FF and photovoltaic efficiency. Furthermore, the FF of the DSSC fabricated with the AgPANI-7 CE (0.629) is higher than the PANI CE (0.547) but lower than that of Pt CE (0.703). This can be ascribed to its lower R_{ct} values (2.15) than the PANI CE (2.41) but higher than Pt CE (2.14), still the DSSC with Ag/PANI-7 CE exhibits a higher cell efficiency of 7.31 % greater than Pt CE (6.84 %) due to its enhanced J_{Sc} value. The conversion efficiency increases with increase in silver concentration and attains a maximum value when concentration is 0.07 M. As a result of these observations, the efficiency enhancement is regarded to the advancement of J_{sc} and FF. For DSSCs using Ag/PANI CEs, the photovoltaic efficiency shows the order of AgPANI-7 > AgPANI-10 > AgPANI-5 > AgPANI-3 > PANI. The AgPANI-7 CE-based solar cell has the highest photovoltaic efficiency of 7.31 %. This photovoltaic efficiency is greater than other polyaniline composites-based CE reported by Lee et al. [26], Hsu [17], Peng [25], and Xiao [56], demonstrating that Ag/PANI composite is a favorable alternate as a CE for DSSCs.

Conclusions

In summary, PANI and Ag/PANI composite CEs are successfully fabricated on stainless steel 304 substrate by electropolymerization using different concentrations of silver. Main advantages of using Ag/PANI composite CEs are high electrical conductivity and large surface area. Electrochemical measurements reveal increased electrocatalytic activity and low charge transfer resistance of the Ag/PANI CEs that improve the photoelectric performance of the DSSCs. The DSSC based on Ag/PANI composite CE achieved a photovoltaic efficiency up to 7.31 %, which is greater than that of DSSC based on Pt CE (6.84 %). The

above discussion demonstrates that Ag/PANI composite is a favorable candidate to replace Pt CE for commercialization of DSSCs.

References

1. Singh PK, Kim KW, Rhee HW (2009) Ionic liquid (1-methyl 3-propyl imidazolium iodide) with polymer electrolyte for DSSC application. Poly Eng Sci 49:862–865
2. Regan BO, Grätzel M (1991) A low-cost, high-efficiency solar cell based on dye-sensitized colloidal TiO2 films. Nature 353:737–740
3. Grätzel M (2003) Dye-sensitized cells. J Photochem Photobiol C 4:145–153
4. Tu CW, Liu KY, Chien AT (2008) Enhancement of photocurrent of polymer-gelled dye-sensitized solar cell by incorporation of exfoliated montmorillonite nanoplatelets. J Polym Sci 46:47–53
5. Li Q, Wu J, Tang Q (2008) Application of microporous polyaniline counter electrode for dye-sensitized solar cells. Electrochem Comm 10:1299–1302
6. Wu J, Li Q, Fan L (2008) High-performance polypyrrole nanoparticles counter electrode for dye-sensitized solar cells. J Power Sources 181:172–176
7. Kay A, Grätzel M (1996) Low cost photovoltaic modules based on dye sensitized nanocrystalline titanium dioxide and carbon powder. Sol Energy Mater Sol Cells 44:99–117
8. Ramasamy E, Lee WJ, Lee DY, Song JS (2008) Spray coated multi-Walled carbon nanotube counter electrode for tri-iodide (I_3^-) reduction in dye-sensitized solar cells. Electrochem Commun 10:1087–1089
9. Pringle JM, Armel V, Mac DR (2010) Electrodeposited PEDOT-on-plastic cathodes for dye-sensitized solar cells. Chem Commun 46:5367–5369
10. Lee KS, Lee HK, Wang DH, Park NG, Lee JY, Park OO, Park JH (2010) Dye sensitized solar cell with Pt- and TCO- free counter electrodes. Chem Commun 46:4505–4508
11. Xiao Y, Lin J-Y, Jihuai W, Tai S-Y, Yue G, Lin T-W (2013) Dye-sensitized solar cells with high-performance polyaniline/multi-wall carbon nanotube counter electrodes electropolymerized by a pulse potentiostatic technique. J Power Sources 233:320–325
12. Jeon SS, Kim C, Ko J, Im SS (2011) Spherical polypyrrole nanoparticles as a highly efficient counter electrode for dye-sensitized solar cells. J Mater Chem 21:8146–8151

13. Ikeda N, Miyasaka T (2006) Conductive polymer–carbon–imidazolium composite: a simple means for constructing solid-state dye-sensitized solar cells. Chem Commun 16:1733–1735

14. Huang KC, Huang JH, Wu CH, CY L, Chen HW, Chu CW, JT L, Lin CL, Ho KC (2011) Nanographite/polyaniline composite films as the counter electrodes for dye-sensitized solar cells. J Mater Chem 21:10384–10389

15. Chen J, Li B, Zheng J, Zhao J, Jing H, Zhu Z (2011) Polyaniline nanofiber/carbon film as flexible counter electrodes in platinum free dye sensitized solar cells. Electrochim Acta 56:4624–4630

16. Xiao Y, Lin JY, Tai SY, Chou SW, Yue G, Wu J (2012) Pulse electropolymerization of high performance PEDOT/MWCNT counter electrodes for Pt-free dye-sensitized solar cells. J Mater Chem 22:19919–19925

17. Hsu Y-H, Chen G-L, Lee R-O (2014) Graphene oxide sheet-polyaniline nanocomposite prepared through in situ polymerization/deposition method for counter electrode of dye-sensitized solar cell. J Polym Res 21:440–448

18. Diarmid AG, Angew (2001) Synthetic metals: a novel role for organic polymers. Chem Int Edit 40:2581–2590

19. Kang ET, Neoh KG, Tan KL (1998) Polyaniline: a polymer with many interesting intrinsic redox states. Polym Polym Sci 23:277–324

20. Li Z, Ye B, Hu X, Ma X, Zhang X, Deng Y (2009) Facile electropolymerized-PANI as counter electrode for low cost dye-sensitized solar cell. Electrochem Commun 11:1768–1771

21. Qin Q, Guo Y (2012) Preparation and characterization of nano-polyaniline film on ITO conductive glass by electrochemical polymerization. J Nanomater. doi:10.1155/2012/519674

22. Xiao Y, Wang W-Y, Wang W-Y, Tai S-Y, Yue G, Wu J (2013) Enhanced performance of low-cost dye-sensitized solar cells with pulse-electropolymerized polyaniline counter electrodes. Electrochim Acta 90:468–474

23. Stejskal J, Gilbert RG (2002) Polyaniline. Preparation of a conducting polymer (IUPAC technical report). Pure Appl Chem 74:857–867

24. Blinova NV, Stejskal J, Trchova M, Prokeš J, Omastova M (2007) Polyaniline and polypyrrole: a comparative study of the preparation. Eur Polym J 43:2331–2341

25. Peng S, Liang J, Mhaisalkar SG, Ramarkrishna SJ (2012) In situ synthesis of platinum/polyaniline composite counter electrodes for flexible dye-sensitized solar cells. Mater Chem 22:5308–5311

26. Lee RH, Chi C-H, Hsu Y-C (2013) Platinum nanoparticle/self-doping polyaniline composite based counter electrodes for dye-sensitized solar cells. J Nanopart Res 15:1733–1747

27. Arup C (2009) Polyaniline/silver nanocomposites: di-electric properties and ethanol vapour sensitivity. Sens Actuators B 138:318–325

28. Safenaz MR, Sheikha M (2012) Synthesis and electrical properties of polyaniline composite with silver nanoparticles. Adv Mater Phy Chem 2:75–81

29. Kumar ABV, Jiang J, Bae CW, Seo DM, Piao L, Kim S-H (2014) Silver nanowire/polyaniline composite transparent electrode with improved surface properties. Mater Res Bull 57:52–57

30. Lan Z, Wu J, Lin J, Huang M, Wang X (2012) Enhancing photovoltaic performance of dye-sensitized solar cells by using thermally decomposed mirror-like Pt-counter electrodes. Thin Solid Films 522:425–429

31. Cheng M, Yang X, Li S, Wang X, Sun L (2012) Efficient dye-sensitized solar cells based on an iodine-free electrolyte using L-cysteine/L-cystine as a redox couple. Energy Environ Sci 5:6290–6293

32. Yan NF, Li GR, Gao XP (2013) Solar rechargeable redox flow battery based on Li$_2$WO$_4$/LiI couples in dual-phase electrolytes. J Mater Chem A 1:7012–7015

33. Tian YG, Huai WJ, Ming XY, Ming LJ, Liang HM, Qing FL, Ying Y (2013) A dye-sensitized solar cell based on PEDOT: PSS counter electrode. Chin Sci Bull 58:559–566

34. Zhou HH, Ning XH, Li SL, Chen JH, Kuang YF (2006) Synthesis of polyaniline–silver nanocomposite film by unsymmetrical square wave current method. Thin Solid Films 510:164–168

35. Stejska J (2013) Conducting polymer–silver composites, REVIEW. Chem Pap 67:814–848

36. Natalia VB, Stejskal J, Trchova M, Sapurina I, Marjanovic GC (2009) The oxidation of aniline with silver nitrate to polyaniline–silver composites. Polymer 50:50–56

37. Mack NH, Bailey JA, Doorn SK, Chen CA, Gau HM, Xu P, Williams DJ, Akhadov EA, Wang HL (2011) Mechanistic study of silver nanoparticle formation on conducting polymer surfaces. Langmuir 27:4979–4985

38. Khanna PK, Singh N, Charan S, Viswanath AK (2005) Synthesis of Ag/Pani nanocomposite via an in situ photo-redox mechanism. Mater Chem Phys 92:214–219

39. Pan LJ, Pu L, Shi Y, Sun T, Zhang R, Zheng YO (2006) Hydrothermal synthesis of polyaniline mesostructures. Adv Funct Mater 16:1279–1288

40. Abdulla HS, Abbo AI (2012) Optical and electrical properties of thin films of polyaniline and polypyrrole. Int J Electrochem Sci 7:10666–10678

41. Peng H, Ma G, Ying W, Wang A, Huang H, Lei Z (2012) In situ synthesis of polyaniline/sodium carboxymethyl cellulose nanorods for high-performance redox supercapacitors. J Power Sources 211:40–45

42. Na Li, Xiao Y, Xu C, Li H, Yang X (2013) Facile preparation of polyaniline nanoparticles via electrodeposition for supercapacitors. Int J Electrochem Sci 8:1181–1188

43. Guptaa K, Janab PC, Meikapa AK (2010) Optical and electrical transport properties of polyaniline–silver nanocomposite. Synth Met 160:1566–1573

44. Carotenuto G (2001) Synthesis and characterization of poly (N-vinylpyrrolidone) filled by monodispersed silver clusters with controlled size. Appl Organomet Chem 15:344–351

45. Carotenuto G, Marletta G, Nicolais L (2001) Dependence of the order-disorder transition temperature of 1-octadecanethiol/silver system on the substrate size. J Mater Sci Lett 20:663–665

46. Amrithesh M, Aravind S, Jayalekshmi S, Jayasree RS (2008) Enhanced luminescence observed in polyaniline polyrnethyl-methacrylate composites. J Alloys Compd 449:176–179

47. Ramesan MT (2014) Synthesis, characterization and properties of new conducting polyaniline/copper sulfide nanocomposites. Polym Eng Sci 54:438

48. R-M J, Bozym D, Punckt C, Aksay I (2010) Functionalized graphene as a catalytic counter electrode in dye-sensitized solar cell. ACS Nano 4:6203–6211

49. Tai Q, Chen B, Guo F, Xu S, Hu H, Sebo B, Zhao XZ (2011) In situ prepared transparent polyaniline electrode and its application in bifacial dye-sensitized solar cells. ACS Nano 5:3795–3799

50. Wang G, Kuang S, Wang D, Zhuo S (2013) Nitrogen-doped mesoporous carbon as low-cost counter electrode for high-efficiency dye-sensitized solar cells. Electrochim Acta 113:346–353

51. Wu M, Lin X, Wang Y, Wang L, Guo W, Qi D (2012) Economical Pt-free catalysts for counter electrodes of dye-sensitized solar cells economical Pt-free catalysts for counter electrodes of dye-sensitized solar cells. J Am Chem Soc 134:3419–3428

52. He B, Tang Q, Wang M, Ma C, Yuan S (2014) Complexation of polyaniline and graphene for efficient counter electrodes in dye-sensitized solar cells: enhanced charge transfer ability. J Power Sources 256:8–13

53. Wang M, Anghel AM, Marsan N-L, Ha C, Pootrakulchote N, Zakeeruddin SM, Grätzel M (2009) CoS supersedes Pt as efficient

electrocatalyst for triiodide reduction in dye-sensitized solar. J Am Chem Soc 131:15976–15977

54. Grätzel M (2005) Solar energy conversion by dye-sensitized photovoltaic cells. Inorg Chem 44:6841–6851

55. Wang G, Xing W, Zhuo S (2012) The production of polyaniline/graphene hybrids for use as a counter electrode in dye-sensitized solar cells. Electrochim Acta 66:151–157

56. Xiao Y, Lin J-Y, Wu J, Tai S-Y, Yue G, Lin T-W (2013) Dye-sensitized solar cells with high-performance polyaniline/multi-wall carbon nanotube counter electrodes electropolymerized by a pulse potentiostatic technique. J Power Sources 233:320–325